6698 *Macromolecules* **2009**, *42*, 6698–6709
DOI: 10.1021/ma900966k

Macromolecules
ARTICLE

Segregation of Carbon Nanotubes/Organoclays Rendering Polymer Blends Self-Extinguishing

Seongchan Pack,*,† Takashi Kashiwagi,§ Daniel Stemp,‖ Jaseung Koo,† Mayu Si,⊥ Jonathan C. Sokolov,† and Miriam H. Rafailovich*,†,‡

†*Department of Materials Science and Engineering,* ‡*Chemical and Molecular Engineering Program, State University of New York at Stony Brook, Stony Brook, New York, 11794-2275,* §*Fire Research Division, National Institute of Standards and Technology, Gaithersburg, Maryland 20899-8665,* ⊥*Venyance Technologies, Inc., Fairlawn, Ohio 44309, and* ‖*North Shore Hebrew Academy High School, Great Neck, New York 11020*

Received May 8, 2009; Revised Manuscript Received July 11, 2009

ABSTRACT: We have shown that the addition of certain nanoparticles mixtures can enhance flame retardancy to a greater degree than the addition of either of the nanoparticles alone. The effect is particularly efficient in polymer blends, where more variables need to be considered in the flame behavior. We studied PS/PMMA blends and the respective homopolymers. In this paper we focused on the combination of multiwall carbon nanoutubes (MWCNTs) with clays. We found that the flame retardant (FR) particles segregate to the MWCNTs preferentially, thereby allowing the clays to segregate to the blend interfaces. In this manner both phase stabilization and good dispersion can be achieved. Both long (0.5−40 μm) and short (1−2 μm) MWCNTs were studied and the results indicated that the *s*-MWCNTs produced the superior flame retardant properties. Addition of all types of nanoparticles, including the standard FR formulations, decreased the time to ignition. On the other hand, the combination of *s*-MWCNT and clay significantly reduced the heat release rate (HRR) and mass loss rate (MLR) relative to compounds with only one type of nanoparticles. Electron microscopy images of the nanocomposites and the chars showed that after heating the *s*-MWCNTs were able to diffuse and form a distinct phase in the nanocomposite. Exclusion of the clays allowed the *s*-MWCNTs to achieve better physical contacts, thereby improving the thermal conductivity. In contrast, the *l*-MWCNTs were entangled and therefore unable to move. The clays formed a barrier between the tube contacts, resulting in an increase of the specific heat and the HRR and MLR relative to the unfilled or the compound with only clays. We therefore conclude that one must consider the organization of nanoparticles, as well as their chemical nature when designing flame retardant nanocomposites, since specific synergies may be established which can reduce the overall concentration of fillers.

1. Introduction

It has recently been demonstrated that the addition of as little as 0.5 wt % multiwalled (MWCNTs) or single-walled carbon nanotubes (SWCNTs) to a polymer matrix can affect the mass loss rate during decomposition, when the nanotubes are well dispersed within the matrix.[1−3] Recently, Kashiwagi et al.[2,3] found that when either 1.0 wt % MWCNTs or 0.5 wt % SWCNTs was added to poly(methyl methacrylate) homopolymer, continuous network-like protective layers were formed. Hence they hypothesized that the network-like layers were to be the factor responsible for the reduction in the mass loss rate (MLR) between the filled and the unfilled homopolymers.[1,4] In an earlier work, Si et al.[5] reported an increase in the flame retardant properties of PMMA when functionalized clays were added. This phenomenon was attributed to the long ribbon-like structures which formed spontaneously when the surfactants on the surfaces of the clays evaporated during heating. Later, they reported that when both the flame retardant (FR) additives and clay nanoparticles were added, a synergy was established where the heat release rate (HRR) and MLR were reduced by more than half as compared to the neat homopolymer.[6]

Recently, Pack et al.[7] have shown that the synergy can be even greater when applied to polymer blends. In the case of polymer blends, the thermal properties can be very complicated because phase separation occurs continuously with different temperatures of thermal degradation. This thermal behavior is also difficult to predict since the distribution of the components in blends is continuously changing during heating. Pack et al.[7] have argued that the inclusion of large aspect nanoparticles may be one solution to predict thermal responses in morphology of polymer blends since it was previously shown that they segregate to the interfacial regions, thereby stabilizing the blends against further thermal decomposition. Furthermore, since the FR particles adsorbed on the surfaces of the clay platelets, the high aspect ratio platelets also functioned as dispersants of the FR particles. The optimal clay loading to achieve these properties was approximately 10% by weight, which is also sufficient to embrittle the polymer matrix and impact the ductility and fracture toughness. Since carbon nanotubes also have a high aspect ratio and an affinity for the flame retardant components, we therefore postulate that an additional synergy may exist when the two types of nanoparticles are combined. This would allow us to obtain superior flame retardant properties, but at a much lower particle loading and hopefully better mechanical properties. Since the aspect ratio of the MWCNTs is much larger than that of the clays, a much smaller loading can yield the mechanical properties which prevent dripping in the molten phase, without embrittlement in the solid phase.

Hence we decided to focus on PS and PMMA homopolymers and their blends, since they already were well characterized and the results could be directly compared to those already in the

*Corresponding author. E-mail: (M.H.R.) mrafailovich@notes.cc.sunysb.edu; (S.P.) spack@ic.sunysb.edu. Telephone: (631) 632-2843. Fax: (631) 632-5754.

 Published on Web 07/31/2009

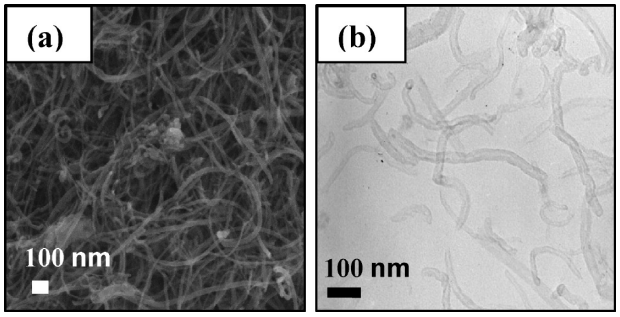

Figure 1. (a) SEM image of *l*-MWCNTs (b) TEM image of *s*-MWCNTs.

literature using Cloisite clays alone.[4,7−9] We then used a series of complementary techniques, in order to determine the relationship between the thermal properties, as measured by cone calorimeter, differential scanning calorimetry (DSC), and thermogravimetric analysis (TGA), with the blend and char microstructures as determined by transmission electron microscopy (TEM), energy dispersive X-ray spectroscopy (EDXS), scanning electron microscopy (SEM), and rheology, as determined by dynamic mechanical analysis (DMA).

2. Experimental Section

Materials and Nanocomposites Preparation. The multiwall carbon nanotubes (MWCNTs) were purchased from Helix Material Solutions, Inc. The lengths of the MWCNTs used in this study were 0.5−40 μm purchased as a long carbon nanotube (*l*-MWCNT) and 1−2 μm as a short carbon nanotube (*s*-MWCNT) in the same diameter, 10−30 nm. (The product IDs of the long and short MWCNTs were MWNT-12950030−00 and MWNT-129500−01, respectively. The batch numbers of both MWCNTs were BMCC05510017 and BMCC05510001.) Electron microscopy images of both types of MWCNTs were shown in Figure 1. Polystyrene (PS) with an average molecular weight of 280K, and poly(methyl methacrylate) (PMMA) with an average molecular weight of 120K, were purchased from Sigma Aldrich. Cloisite 20A was provided by Southern Clay Products Inc. The flame retardant (FR) compound was decabromodiphenyl ether (DB), purchased from Sigma Aldrich and the synergist, antimony trioxide, Microfine AO3, (AO) was purchased from Great Lakes Chemical Corporation. A C.W. Brabender instrument, type EPL-V501, with a direct current drive (type GP100) was used to blend the nanocomposites. The blender was equipped with two screw-type roller blades in a heating chamber. The polymer pellets were first added to the chamber at a rotation speed of 20 rpm and temperature of 170 °C. The FR agents were then inserted and mixed at the same rpm for 2 min. Either the MWCNTs or the Cloisite 20A clay was gradually added into the chamber, while blending. The entire mixture was blended at 100 rpm for 15 min under nitrogen gas flow, which prevented degradation of the mixture from heat-induced oxidation. The mixture was allowed to cool at room temperature in the chamber, and then small pieces of the mixture were molded in a hot press into the different shapes required for the various mechanical tests and flame tests that were performed.

Flammability Measurements. The heat release rate (HRR) and mass loss rate (MLR) measurements of each sample were performed using cone calorimetry at the National Institute of Standards and Technology (NIST). The samples were made by molding 24 ± 2 g of the composite into a 75 mm × 75 mm × 5 mm square. The samples were then wrapped on three sides with thin aluminum foil, exposing one side in the direction of the thermal radiation. The samples were exposed, in ambient atmosphere, to an external radiant flux of 50 kW/m^2, normal to the sample surface and the HRR and MLR were measured as a function of exposure time. The residues in the thin aluminum foiled containers were collected and their morphology was characterized by scanning electron microscopy (SEM). The standard uncertainty of the measured heat release rate (HRR) was ± 10%. The cone calorimetry test was conducted by ASME/ISO 5660.

Table 1. Results of UL-94 V0 Test from Nanocomposites

sample (concentration, wt %)	dripping	UL-94 VO	sample burning total time ($t_1 + t_2$), s
PMMA(100)	yes	NG[a]	
PMMA/DB/AO(75/20/5)	yes	NG	
PMMA/DB/AO/*l*-MWCNTs-(75/20/5/0.5)	no	V0	< 10
PMMA/DB/AO/*l*-MWCNTs-(75/20/5/1.5)	no	V0	< 10
PS/PMMA(70/30)	yes	NG	
PS/PMMA/DB/AO(70/30/15/4)	yes	NG	
PS/PMMA/DB/AO/Cloisite 20A(70/30/15/4/3)	no	NG	
PS/PMMA/DB/AO/Cloisite 20A/*l*-MWCNTs(70/30/15/4/3/2)	yes	V2	< 10
PS/PMMA/DB/AO/Cloisite 20A/*s*-MWCNTs(70/30/15/4/3/2)	no	V0	< 10

[a] NG: No grading and burnt up to the upper clamp at the stand.

UL-94 V0 Test. A vertical burning chamber purchased from Underwriters Laboratories Inc. was used to assess flammability. Samples of dimensions 125 mm × 13 mm × 1.5 mm were molded and tested using the protocol established by ASTM D3801/ISO 1210 UL 94 V0. The test to probe flame retardancy was conducted by first clamping the samples approximately 10 mm from the top edge and suspending them, with the long axis pointing down, from a ring stand. A compressed methane gas burner with a gas flow rate of 105 mL/min was then placed 20 mm beneath the lower edge of the samples. A flame, 20 ± 2 mm, high was applied to the sample for 10 s and then t_1, the time that it took to extinguish the flame, was measured. The flame was then reapplied and t_2, the time to extinguish the flame again, was measured. If either t_1 or t_2 was less than 10 s, then the sample was classified as V0 in the UL-94 test. Furthermore, it was also recorded whether the nancomposites dripped and/or ignited a wad of cotton placed under the holder. Table 1 shows the results of the UL-94 V0 test from nanocomposites.

Morphology of Nanocomposites. In order to analyze the internal structures before and after exposure to the flame, transmission electron microscopy (TEM) and scanning electron microscopy (SEM), were used to characterize the morphology of samples. Transmission electron microscopy (TEM) was conducted with cross sections of samples obtained from before or after the vertical burning test. In particular, the vertically burned samples were cut into three parts. The first piece was taken from the bottom of the sample, which was closest to the flame. The second one was chopped 30 mm away from the first cut in the sample. The last one was obtained 30 mm away from the second cut in the same sample. The cross sections were cut to a thickness of 70−80 nm using the Reichert-Jung Ultracut E ultramicrotome and then they were floated at the water surface on coated copper mesh grids. Morphology of the cross sections was viewed from a FEI Tecnai12 BioTwinG^2 TEM at 80 kV and digital images were acquired with an AMT XR-60 CCD digital camera system.

The elemental distribution of Br, or the flame retardant agent was imaged using an energy dispersive X-ray spectroscopy (EDXS) attachment on the SEM (LEO-1550) with a Schottky field-emission gun. The SEM/EDXS measurements were conducted on (5 mm × 5 mm × 2 mm) samples that were heated for different times in air at a temperature of 650 °C in a Lindberg SB type 167 oven chamber. The SEM was also conducted with the residues after the cone calorimetry test in air. A few micrometers of gold were coated on the surface of the residues in order to make the specimens conduct.

Thermodynamic and Thermal Stability Measurements. Dynamic modulus of the samples was measured by a Mettler

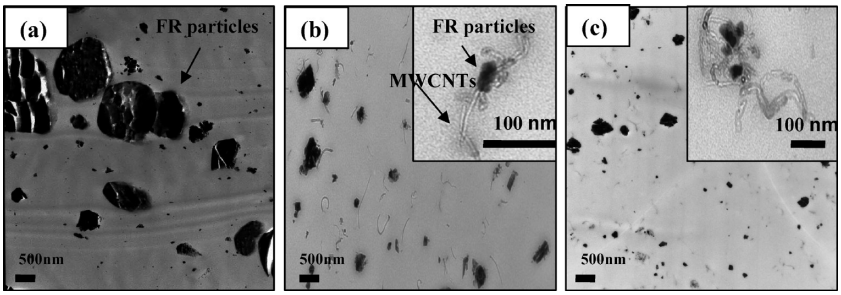

Figure 2. TEM images: (a) PMMA/DB/AO(75/20/5 wt %), (b)PMMA/DB/AO/*l*-MWCNT(75/20/5/0.5 wt %), and (c) PMMA/DB/AO/*s*-MWCNT(75/20/5/0.5 wt %).

Toledo DMA/SDT 861e in the single cantilever mode. Elastic modulus and tan delta of samples, molded into bars of dimension 10 mm × 10 mm × 2 mm, were measured as a function of temperature, where the temperature was raised from room temperature to 180 °C at a rate of rate 2 °C /min from room temperature at a frequency of 1 Hz.

A differential scanning calorimeter (DSC) was used to calculate the specific heat of chars. The DSC measured the heat flow of the char as a function of time and temperature. In order to correctly determine the specific heat, the mass of the samples is required and then input into the formula:[18]

$$C_p = \frac{\Delta H}{\Delta T \times M} = \left(\frac{\mathrm{d}H}{\mathrm{d}t}\right)\left(\frac{\mathrm{d}t}{\mathrm{d}T}\right)\left(\frac{1}{M}\right)$$

,where ΔH is the enthalpy change, ΔT is the temperature change, $\mathrm{d}H/\mathrm{d}t$ is the heat flow difference between the blank and the sample, $\mathrm{d}t/\mathrm{d}T$ is the reverse of the heating rate (20 °C /min), and M is the mass of the sample. Thermogravimetric analysis (TGA) was performed using a Mettler-Toledo 2000 analyzer in order to determine the time/temperature sequence of mass loss in the decomposition. A small mass of a sample (10−15 mg) was measured and then inserted into an aluminum crucible. The crucible with the sample was put at the small dish in the furnace and then the temperature was increased from 30 to 800 °C at a rate of 10 °C/min. The TGA data was normalized in a percentage of mass loss and the first derivative of the spectrum was obtained in order to clearly indicate the transition points. Rheology measurements were carried out using a Bohlin Gemini HR Nano rheometer from Malverm instruments. A constant strain amplitude (0.5%) was applied for frequency sweep ($0.01 < \omega < 100$ Hz) in oscillatory shear. All samples were run at 200 °C on a 20 mm under the flow of nitrogen to avoid degradation of the samples.

3. Results and Discussions

Morphology of Microstructures in Nanocomposites. *Homopolymer Nanocomposites*. TEM cross sections from the nanocomposites are shown in Figure 2. From the figure we can see that both short and long MWCNTs are well dispersed in PMMA/DB/AO matrix by melt blending. The FR particles, which are electron dense and appear darker in color than the surrounding polymer matrix, are also seen to be much better dispersed when the MWCNTs are present. Analysis of the average FR particle size indicates that, in the absence of MWCNT's, large, microscale particles are present, with a mean size of 2 ± 0.5 μm. Addition of the MWCNTs is seen to dramatically decrease the size of the particles to 500−300 nm or 300−50 nm when *l*-MWCNTs or *s*-MWCNTs are added, respectively. In the inset we show higher magnification TEM images where we can see that the FR particles are preferentially attracted to the MWCNT surfaces, which increases their dispersion in the matrix. A similar result was also reported by Si et al. for the PMMA/DB/AO nanocomposites when Cloisite 20A were added.[6]

In order to determine the effects of the dispersion on the mechanical properties of the polymer we also performed DMA and rheology tests. In Figure 3a we show the tan delta plots of the nanocomposites, where we can see that the addition of either MWCNTs or FR particles increases T_g of the matrix from 125 °C to around 136 or 138 °C, respectively. However, the addition of both types of the MWCNTs together with the FR particles increases T_g of the matrix by 15 to 140 °C. This indicates that strong interactions exit between the matrix polymer chains and both the FR and the MWCNT particles. The slight additional increase in T_g when both particles are added can be explained by the additional surface area created for polymer adsorption sites when the diameter of the FR particles is decreased even further caused by the adsorption of FR particles onto the MWCNT surfaces. Hence, when PMMA is blended with other polymers, both the FR particles and MWCNTs will likely be segregated in the PMMA phase. Furthermore, the ability of the MWCNTs to better disperse the FR particles produces the synergy to which the enhanced mechanical properties shown in Figure 3 can be attributed. In Figure 3b we also plot the storage modulus of the nanocomposites formed with *s*-MWCNTs or *l*-MWCNTs and PMMA/DB/AO matrix, together with data for the unfilled PMMA matrix and the matrix with just the MWCNTs without the FR particles. From the figure we can see that the modulus of either the *l*-MWCNTs or *s*-MWCNTs filled nanocomposite samples are reduced about 20% as compared to the modulus of pure PMMA sample for $T < 90$ °C. Above that temperature the modulus of both the MWCNTs increase, which would predict the enhancement of impact toughness when the carbon nanotubes are added. The addition of FR particles (25% by weight) increases the magnitude of the modulus by 35% relative to that of pure PMMA. This may lead to an increase of brittleness and would reduce the impact toughness. However, the addition of both types of particles; FRs (25 wt %) and MWCNTs (0.5 wt %) increases the modulus by 70% relative to that of pure PMMA for $T < 90$ °C. This increase of the modulus may produce overall a tougher material.[19] In Figure 4 we show the elastic modulus versus frequency plots for the PMMA nancomposites. From the figure we see that the addition of 0.5 wt % MWCNTs produces only a slight enhancement of the storage modulus, in agreement with the previous results of Kashiwagi[2] with only a negligible difference between the long and short nanotubes. The addition of FR particles to PMMA increases the modulus by a factor of less than half. On the other hand, the addition of both FR and MWCNTs particles produces a dramatic increase by nearly one and half orders of magnitude at frequencies below 1 Hz. This indicates that by themselves, either low concentrations of MWCNTs or FR particles produce a network structure. On the other hand, together, they also establish

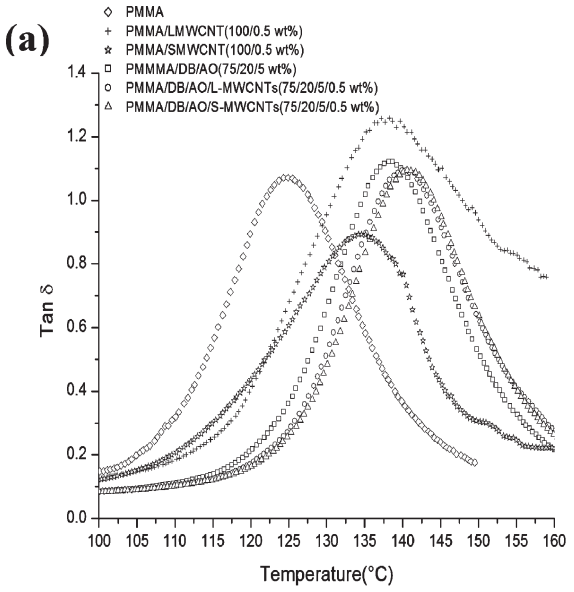

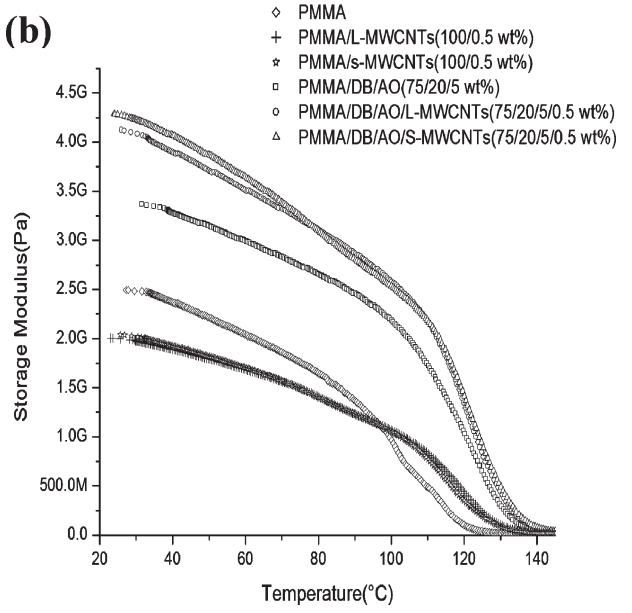

Figure 3. Storage modulus and tan δ vs temperature curves: PMMA, unfilled diamond; PMMA/*l*-MWCNT(100/0.5 wt %), unfilled cross; PMMA/*s*-MWCNT(100/0.5 wt %), unfilled star; PMMA/DB/AO(75/20/5 wt %), unfilled square; PMMA/DB/AO/l-MWCNT(75/20/5/0.5 wt %), unfilled circle; PMMA/DB/AO/*s*-MWCNT(75/20/5/0.5 wt %), unfilled triangle.

a synergy in the dynamical properties corresponding to the formation of internal networks. The percolation of the networks at smaller MWCNTs concentrations may also be due to the strong interactions with the matrix by the DB/AO particles and the increased surface area available for the adsorption of polymer chains, which is a result of the improved dispersion. Network formations were previously reported to correlate with improved flame retardant properties, due to the improved structure of the char layer. In the previous case, the improvements were observed only after the addition of at least 2% MWCNTs. This was the minimum concentration of MWCNTs which formed a dense network, smooth char layers, and the reduced MLR. In our case, the combination of particles produces an even larger decrease in the HRR, which is not surprising given

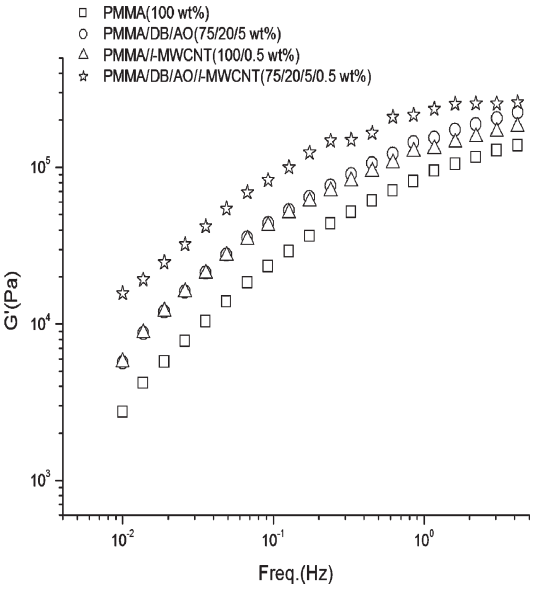

Figure 4. G' vs frequency curves: PMMA, unfilled square; PMMA/DB/AO(75/20/5 wt %), unfilled circle; PMMA/*l*-MWCNT(100/0.5 wt %), unfilled triangle; PMMA/DB/AO/*l*-MWCNT(75/20/5/0.5 wt %), unfilled star.

the UL-94 V0 response to heating in an open flame. Hence the superior flame retardant properties can be also being directly attributed to the synergy with the MWCNT that produces the enhanced dispersion of the FR particles. In Figure 5, we show a series of TEM images taken from segments obtained at different distances from a flame. From the figure we can see that the dispersion of both MWCNTs and FR particles is similar in all frames, indicating that it is not affected by the flame, which was applied during the UL-94 V0 testing time of 20 s. The network formed by the MWCNT prevented the polymer/DB/AO melt from dripping, while the FR particles remained uniformly distributed, since it was adsorbed to the nanotubes, and did not flow with the polymer.

Polymer Blends Nanocomposites. Improving the flame retardant properties in immiscible polymer blends is considerably more complex than in homopolymers. In this case, the polymer/ FR composites form a complicated three phase system with unpredictable behaviors when heat is applied. We have previously shown that the addition of 5% Cloisite 20A to PS/PMMA/DB/AO system can stabilize the system against further phase segregation and disperse the FR particles inside the PMMA phase, which resulted in improved flame retardant properties such as the reduced MLR and HRR, (and passing the UL-94 V0 test). Si et al.[10] had also shown previously that clays added to immiscible polymer blends can form *in situ* grafts which segregate to the polymer interfaces and promote compatibilization. When the FR formulation was added though, the FR also segregated to the clay surfaces, displacing the polymer and interfering with the ability of the clays to act as interfacial tension reduction agents.[7] We have also shown previously that other large aspect ratio particles can also compatibilize polymer blends.[13] Hence, we postulated that the addition of MWCNTs may enhance the compatibilization of the blend and thereby improve its thermal and rheolocical properties, while decreasing the total concentration of particle additives. We therefore reduced the amount of Cloisite 20A clay from 10% to 3% and added 2% MWCNTs. TEM cross sections of the nanocomposites blended with *l*-MWCNT and *s*-MWCNT are shown in Figure 6, which is included with the image of

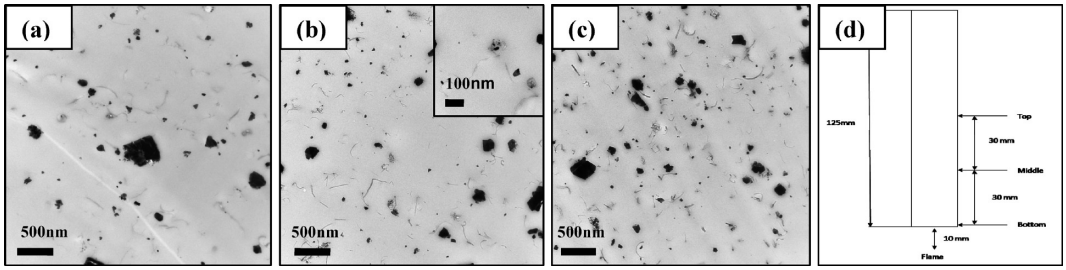

Figure 5. TEM images obtained from a nanocomposite bar that was heated in a flame for the UL-94-V0 test: (a) top, (b) middle, and (c) bottom of PMMA/DB/AO/*l*-MWCNT(70/25/5/0.5 wt %) and (d) scheme of UL-94 V0 set.

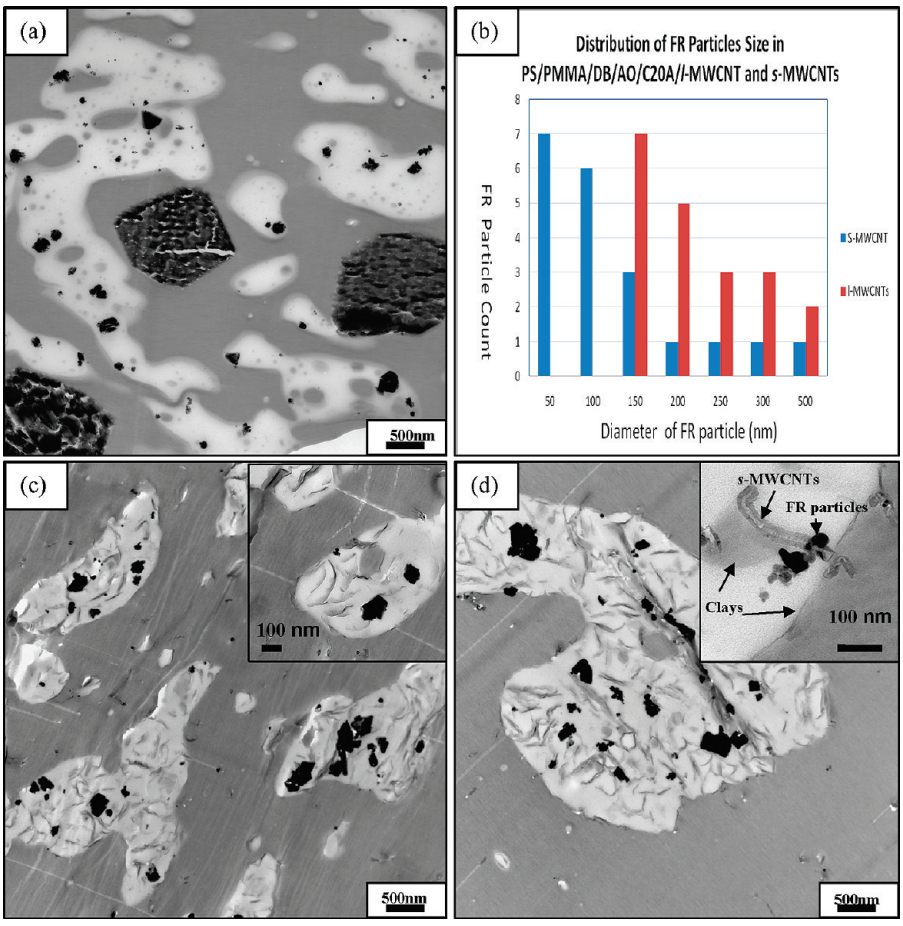

Figure 6. TEM images: (a) PS/PMMA/DB/AO (70/30/15/4 wt %), (b) Distribution of FR particles size in PS/PMMA/DB/AO/Cloisite 20A/l-MWCNT and s-MWCNT (c) PS/PMMA/DB/AO/Cloisite 20A/*l*-MWCNT (70/30/15/4/3/2 wt %), (d) PS/PMMA/DB/AO/Cloisite 20A/*s*-MWCNT (70/30/15/4/3/2 wt %).

cross-section obtained from the polymer blend without the nanoparticles additives. From the figure we can see that the FR particles segregate in the PMMA phase, while the clays, which also segregate in the PMMA phase, are present at the interfaces. Comparing the images of the *s*-MWCNTs with those from the *l*-MWCNTs, we find that the FR particle size is significantly smaller in the blend with the *s*-MWCNTs, which is shown in Figure 6b. Furthermore, we find that in the case of the *s*-MWCNTs, all tubes are present both in PMMA and PS phases, while in the case of *l*-MWCNTs most of the tubes are in PS phase. In the inset, we show a higher magnification images where we can more clearly resolve the MWCNTs. From the images, we can see that the FR particles are preferentially segregated on the *s*-MWCNT rather than the clay surfaces. The presence of some of the *s*-MWCNTs in the PMMA phase then assists in the dispersion of the particles. Furthermore, as can be seen in the figure, the clay platelets are again localized at the polymer interfaces, as previously shown by Si et al.,[10] since no FR particles are present to screen the surface interactions. The surface interactions also impact the rheological properties of the blend. In Figure 7 we show the DMA data obtained for the polymer blends with FR particles, Cloisite 20A, and both types of MWCNTs. The moduli at $T = 50$ °C and the values of T_g obtained from the tan δ measurements are tabulated in Table 2. From the table we can see that the addition of FR particles to the blend lowers the modulus by nearly 26%. In the case of the homopolymer FR particles increased the T_g of the compound indicating that they interacted favorably with the matrix, and the increased interfacial adhesion with the inorganic particles enhanced the mechanical strength of the microcomposite. In the case of immiscible polymers, the

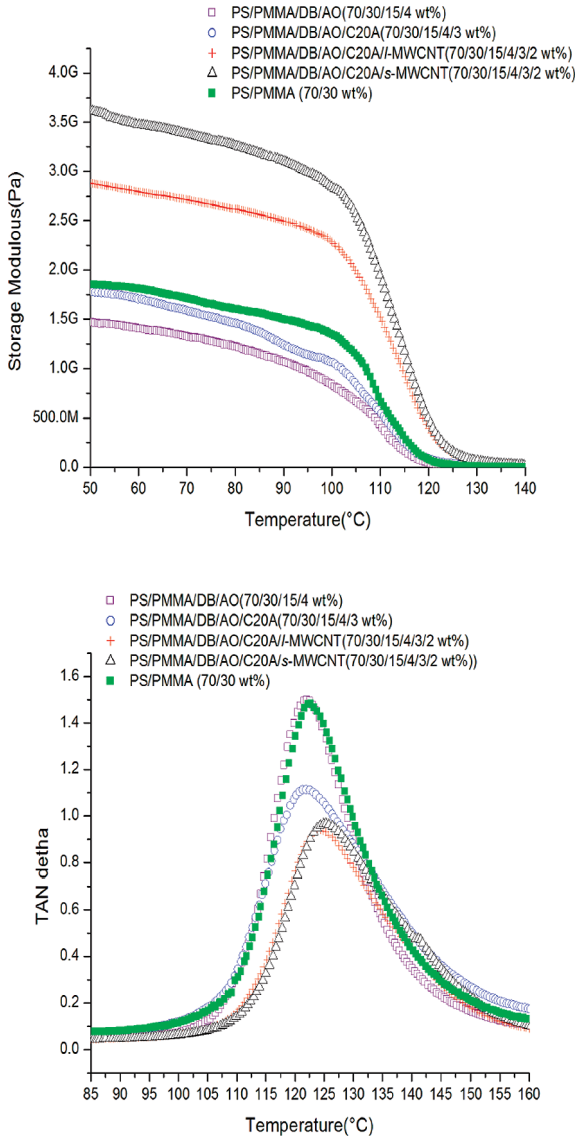

Figure 7. Storage modulus and tan δ vs temperature curves: PS/PMMA/DB/AO(70/30/15/4 wt %), unfilled purple square; PS/PMMA/DB/AO/Cloisite 20A (70/30/15/4/3 wt %), unfilled blue circle; PS/PMMA/DB/AO/Cloisite 20A/*l*-MWCNT (70/30/15/4/3/2 wt %), unfilled red cross; PS/PMMA/DB/AO/Cloisite 20A/*s*-MWCNT(70/30/15/4/3/2 wt %), unfilled black triangle; PS/PMMA (70/30 wt %), filled green square.

unfavorable interactions between the two components decrease the interfacial penetration between domains which reduces the mechanical integrity of the blend.[13] The FR segregates exclusively into the PMMA domains and hence do not reinforce the blend. In fact an increased T_g is likely to be accompanied by a decreased diffusion coefficient and as has been previously observed for carbon nanoparticles in a PB blend, decreases the interfacial width between domains.[13] This phenomenon would be consistent with the further decrease in modulus resulting from addition of the FR particles. Addition of the Cloisite clays somewhat restores the modulus of unfilled blend since, as was previously shown, the clay platelets are positioned at the blend interfaces, reducing the interfacial tension. But, as was shown in ref 7, when FR particles are present, they compete with the polymer chains for the clay surfaces, thereby reducing the efficiency of the clay to form grafts and reduce the interfacial tension. A significant improvement is observed when the

Table 2. Results of Rheological Properties from PMMA/MWCNTs Nanocomposites and PMMA/DB/AO without MWCNTs and with MWCNTs Nanocomposites

sample (concentration, wt %)	T_g(°C)	E' (GPa) at T = 35 °C
PMMA (100)	125	2.44
PMMA /*l*-MWCNTs (100/0.5)	138	1.93
PMMA/*s*-MWCNTs (100/0.5)	135	1.97
PMMA/DB/AO (75/20/5)	138	3.34
PMMA/DB/AO/*l*-MWCNTs-(75/20/5/0.5)	140	3.98
PMMA/DB/AO/*s*-MWCNTs-(75/20/5/0.5)	140	4.15
sample (concentration, wt %)	T_g(°C)	E' (GPa) at T = 50 °C
PS/PMMA (70/30)	122.7	1.85
PS/PMMA/DB/AO (70/30/15/4)	122	1.47
PS/PMMA/DB/AO/C20A (70/30/15/4/3)	121.9	1.77
PS/PMMA/DB/AO/C20A/*l*-MWCNTs(70/30/15/4/3/2)	124.3	2.87
PS/PMMA/DB/AO/C20A/*s*-MWCNTs(70/30/15/4/3/2)	125.3	3.61

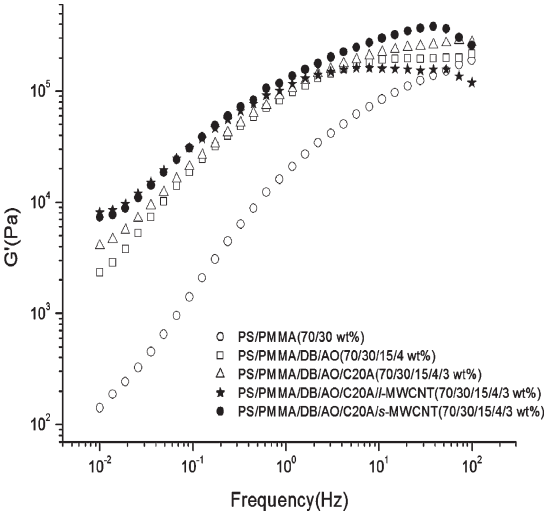

Figure 8. G' vs frequency curves: PS/PMMA (70/30 wt %), unfilled circle; PS/PMMA/DB/AO(70/30/15/4 wt %), unfilled square; PS/PMMA/DB/AO/Cloisite 20A (70/30/15/4/3 wt %), unfilled triangle; PS/PMMA/DB/AO/Cloisite 20A/*l*-MWCNT (70/30/15/4/3/2 wt %), filled star; PS/PMMA/DB/AO/Cloisite 20A/*s*-MWCNT(70/30/15/4/3/2 wt %), filled circle.

MWCNTs are added, with the short MWCNTs being even more effective than the long MWCNTs. Examination of Figures 2 and 6 provides a possible explanation for the observed synergy. As we discussed for the case of the homopolymer, the FR particles prefer the carbon nanotube surfaces to those of the clays. Hence even in the blend, the carbon nanotubes are decorated with the FR particles within the PMMA phase domains. As a result, the clay platelets can now form in situ grafts thereby reducing the interfacial tension, improving the adhesion between the components, and increasing the modulus, as was shown by Si et al. for the blend without the FR particles.[10] As a result of the increased interfacial area, the mean size of the FR particles is slightly smaller and the dispersion is improved in case of the addition of short MWCNTs, which is confirmed by the Figure 5b. Hence the major difference between the two types of MWCNTs appears to be in the dynamical response of the matrix to the addition of the tubes. This can further be probed with greater accuracy by comparing the frequency responses of the moduli of the two different types of samples.

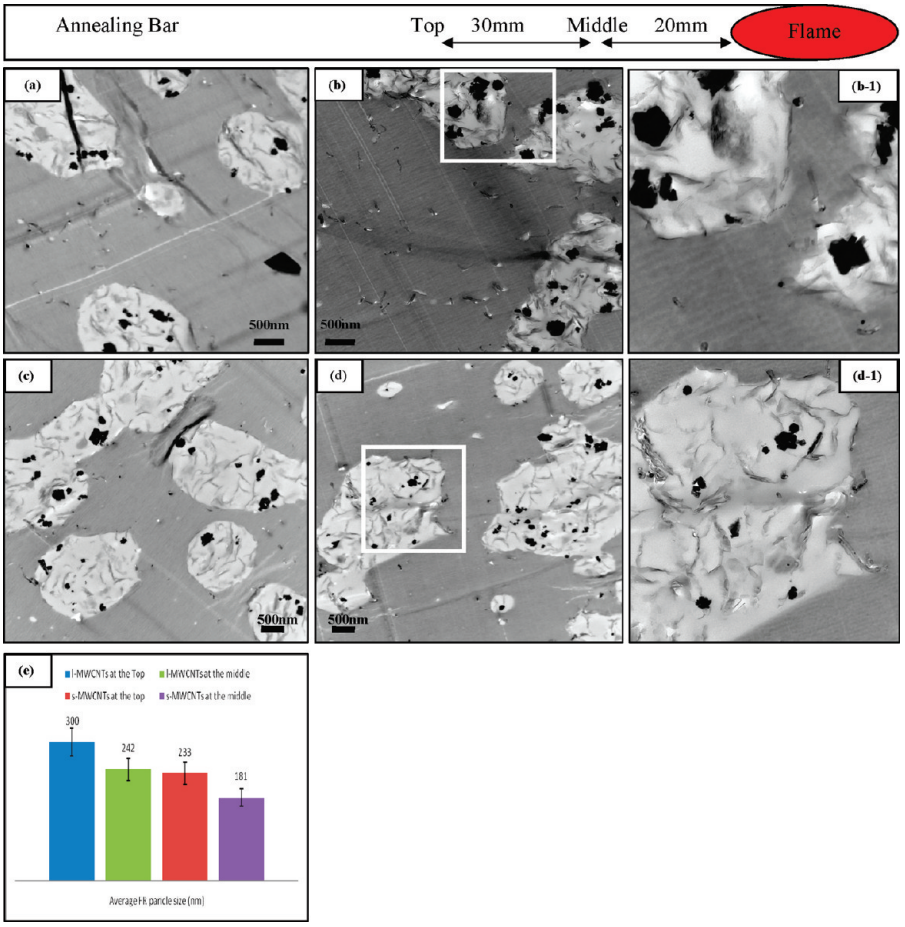

Figure 9. TEM images of two series of *l* and *s*-MWCNTS annealing Bars: (a) top, (b) middle of PS/PMMA/DB/AO/Cloisite 20A/*l*-MWCNTs (70/30/15/4/3/2 wt %) bar and (c) top, (d) middle of PS/PMMA/DB/AO/Cloisite 20A/*s*-MWCNT(70/30/15/4/3/2 wt %). (b-1) and (d-1): Higher magnification TEM images of parts b and d. (e) Mean size of FR particles at each section in both the *l*-MWCNTs and the *s*-MWCNTs.

Rheological Measurements. The frequency dependence of storage modulus also provides a sense of internal dynamics of a polymer blend.[12] In Figure 8 we plot G' vs ω for the different nanocomposites, and compare them to the unfilled polymer blend. From the figure we can see that the overall frequencies the pure polymer blend follows the classical scaling behavior for a ($G' \sim \omega^2$) viscous liquid, as expected at $T = 200$ °C. The temperature is sufficiently high that no plateau is observed even at 100 Hz, indicating that 1/frequency is still long enough that the polymer chains are rearranged in their configuration. When the FR particles is added we find that G' still obeys the liquidlike relationship at low frequencies, but the absolute value is nearly an order of magnitude higher, which is consistent with an increase in "rigidity" due to an increase in T_g caused by the attractive interactions between PMMA phase and the FR particles. The addition of Cloisite 20A with the FR particles does not affect the rheological responses significantly; hence no change has occurred in the polymer dynamics. Even though the Cloisite 20A has previously been shown to decrease the diffusion coefficient of PMMA and hence increase the viscosity,[11] in this case, the clay platelets are covered with the FR particles and hence do not interact effectively with the polymer chains, confirming the observations of Pack et al.[7] A significant change occurs with the addition of MWCNTs. At low frequencies the response with both types of nanotubes is identical. A small flat region is observed initially indicating the formation of a weak network of entanglements. At approximately 1 Hz the response of the samples with the two types of MWCNT begins to diverge. G' for the *s*-MWCNTs continues to increase until about 10 Hz, when a sharp decrease is observed. In the case of the *l*-MWCNT a plateau occurs at 1 HZ, indicating the formation of an entangled network. The plateau extends until 10 Hz when a sharp decline is observed. The sharp decrease in both cases is indicative of a breakdown in the melt at these higher frequencies which occurs only upon introduction of the nanotubes.

Thermal Properties. In order to examine the evolution of the microstructures after flame testing, samples (125 mm × 13 mm × 1.5 mm) of PS/PMMA/DB/AO/Cloisite20A with the *l*-MWCNTs or the *s*-MWCNTs were exposed to a flame as shown in Figure 9 for a total time of 20 s (following the UL-94 V0 test protocol). Each sample of the bar was then divided into two sections. The middle section was 20 mm away from the flame, and the top was another 30 mm away, (or 50 mm) away from the center of the flame as shown in Figure 9 (top). The lowest segment that was in the flame contained mostly char and is not shown. TEM images of the cross sections obtained from the *l*-MWCNTs and the *s*-MWCNTs nanocomposites are shown in Figure 9a,b and Figure 9c,d, respectively. The major difference between the two types of samples is in the distribution of MWCNTs. In the case of the *l*-MWCNTs, a large fraction of the tubes can be seen in PS phase, and this fraction is nearly the same between the top and bottom portions of the sample. In the case of the sample containing *s*-MWCNT, a few nanotubes are seen in the PS phase in the top image, but all the nanotubes are now in PMMA phase in the middle image.

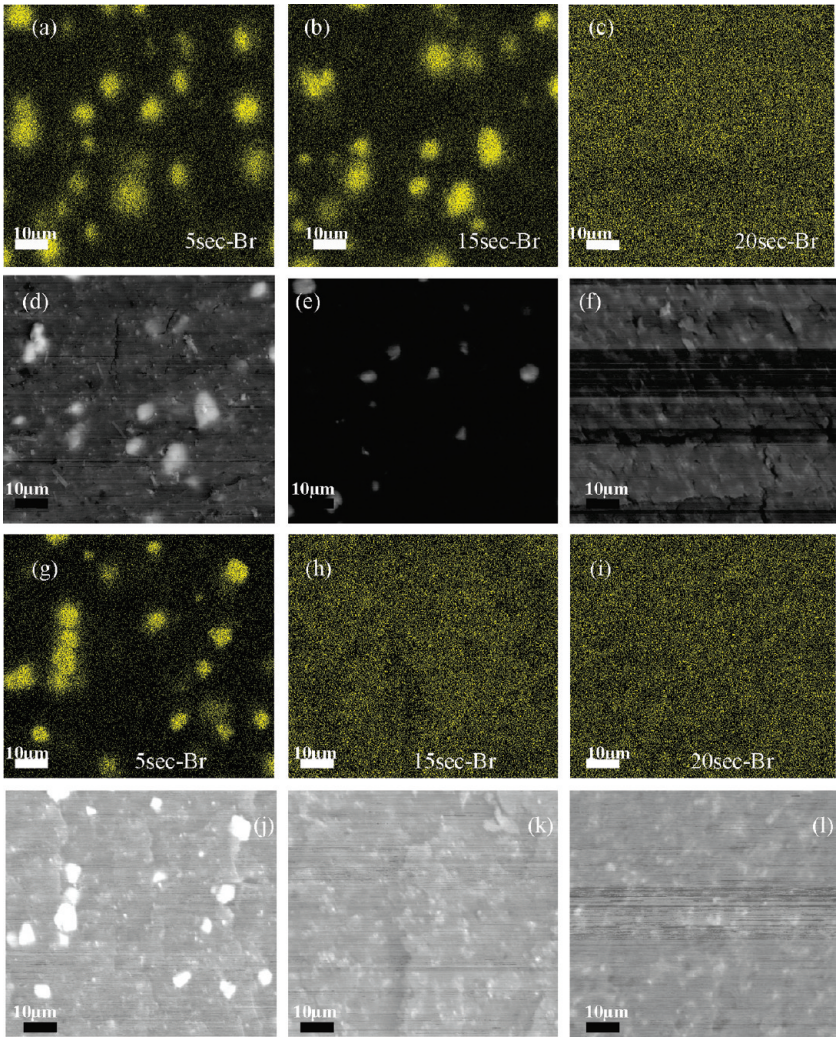

Figure 10. Br mapping and SEM images: (a−f) PS/PMMA/DB/AO/Cloisite 20A/*l*-MWCNT(70/30/15/4/3/2) samples; (g−l) from the PS/PMMA/DB/AO/Cloisite 20A/*s*-MWCNT(70/30/15/4/3/2) samples.

In Figure 9b-1 and Figure 9d-1, we show magnified sections of a PMMA segment in each of the images. Here we can see that in the case of the *l*-MWCNT sample, the FR particles are clustered around clay platelets in the PMMA phase. A few nanotubes can be seen at the PS/PMMA interfacial region, but most tubes remain in the PS phase. In the case of the s-MWCNTs, many the nanotubes can be seen segregated in the PMMA phase, including a large fraction of nanotubes that are at the PS/PMMA interfaces. As shown previously, the FR particles appear adsorbed to the carbon nanotube surfaces, even in the middle segment. In Figure 9e, we also plot the mean FR particle sizes obtained from both types of samples, and compare the sizes in the top and middle segments.

From Figure 9 we can see that the clays in both types of samples have begun to form the characteristic ribbon like structures that were previously reported to form when the samples were heated to the decomposition temperature ($T >$ 250 °C) of the ditallow surfactants on the Cloisite 20A clays. In the top part of the samples, the average FR particle size however did not change significantly from the value found in the unheated samples (Figure 5), indicating that the ambient temperatures in this region were below 350 °C, the decomposition temperature of "decabrom". In both cases we can see that the average particle diameter decreases significantly in the midportion of the samples. The rate of decrease however seems to be significantly larger in the *s*-MWCNTs sample, which is consistent with the smaller initial particle size, where the rate of decrease is a function of both temperature and particle diameter.

Energy Dispersion Analysis X-ray (EDAX). In order to confirm this observation the two types of samples were also imaged using SEM with energy dispersion analysis X-ray (EDAX) mapping which provides elemental specificity for higher Z elements. *l*-MWCNT and *s*-MWCNT samples were heated to 600 °C in air for different times and cross-sectioned. The SEM scans of both samples are shown in Figure 10. From the figure the bright regions correspond to the FR particles which have higher Z than the matrix and scatter more electrons. The yellow images were obtained by setting a window on the Br l-edge peak obtained from the EDAX spectra of the samples and scanning. Since the X-rays come from a broad internal region, the intrinsic spatial resolution of EDAX is approximately 1 μm. Hence, to obtain enough intensity, the scale bar in these images is 10 μm, and the bright regions correspond to entire PMMA *domains* where the FR particles are segregated. From the figure we can see that in the case of the *l*-MWCNTs, the FR domains, are initially bright after heating for 5 s, somewhat less bright after 15 s and disappear 20 s after heating. Hence, the Br is no longer visible after 20 s. In contrast, for the case of the *s*-MWCNT, the bright domains disappear faster, or after 15 s

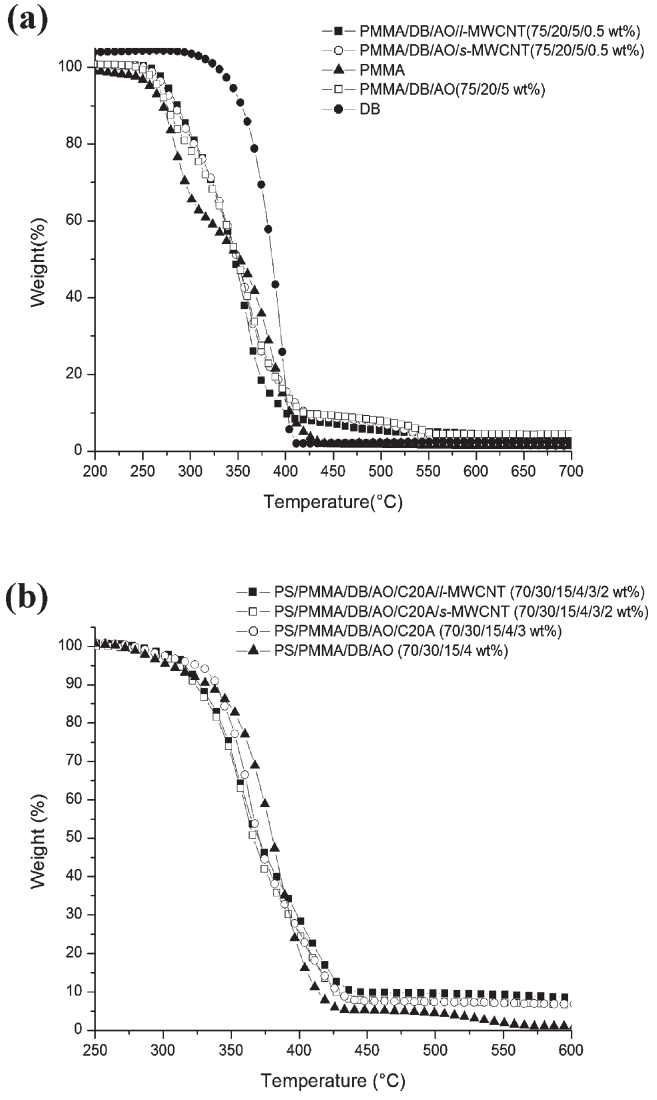

Figure 11. (a) Curves of TGA from the PMMA polymer blends and (b) curves of TGA from the PS/PMMA polymer blends.

of heating, hence the smaller particles are more easily converted to the vapor phase. The more efficient vaporization of Br particles improves the ability of the formulation to act as a flame retardant and react in a vapor phase with the gaseous degradation products of polymers that are emitted sooner than those of the inorganic components.

Thermogravimetric Analysis (TGA). In order to investigate the effects of the nanotubes on the thermal stability of the melt we also performed TGA measurements on the nanocomposites. The results for the homopolymer are shown in Figure 11. In contrast to the results reported in Pack et al., where clay was seen to increase the thermal stability, the addition of MWCNT in PMMA/DB/AO blend appears to be no change in the trace of the blend, which indicates that the addition of MWCNTs mainly act as a physical barrier in the molten polymer matrix. This is also consistent with the results that there was no dripping in the UL94 V0 flame test. Another interesting fact is to note that the decomposition temperatures of both formulations are symmetrically located around the decomposition temperature $T = 350$ °C of DB. Furthermore, we can also see that both formulations have only one decomposition temperature, as opposed to the two step process observed with the PMMA polymer. Hence, the precise order to the decomposition is not as important as the proximity to the decomposition temperature of the DB in facilitating the gas phase reaction which stabilizes the polymer matrix from decomposition, and quenches a flame.

Table 3. Results of Cone Calorimeter of PMMA/DB/AO without the Clay and with the *l*-MWCNTs Nanocomposites

sample (concentration, wt %)	peak HRR (kW/m^2)	average MLR (g/s)	ignition time (s)
PMMA (100)	1440.9	0.138	25 ± 1
PMMA/DB/AO (75/20/5)	490.4	0.177	15 ± 2
PMMA/DB/AO/ *l*-MWCNTs(75/20/5/0.5)	436.7	0.172	5 ± 1
PMMA/DB/AO/ *l*-MWCNTs(75/20/5/1.5)	377.8	0.128	10 ± 1

Table 4. Results of Cone Calorimeter of PS/PMMA/DB/AO with the Clay and with the Clay and the MWCNTs Nanocomposites

sample (concentration, wt %)	peak HRR (kW/m^2)	average MLR (g/s)	ignition time (s)
PS/PMMA (70/30)	1507.8	0.137	25 ± 1
PS/PMMA/DB/AO(70/30/15/4)	570.0	0.131	18 ± 2
PS/PMMA/DB/AO/Cloisite20A (70/30/15/4/3)	375.0	0.107	18 ± 2
PS/PMMA/DB/AO/Cloisite20A/ *l*-MWCNTs (70/30/15/4/3/2)	338.4	0.113	15 ± 2
PS/PMMA/DB/AO/Cloisite20A/ *s*-MWCNTs (70/30/15/4/3/2)	307.7	0.095	12 ± 2

The effect is even more dramatic in the case of the blend. Here we find that the addition of PS moves the degradation temperature of the blend to $T = 375$ °C, which is significantly higher than that of the DB. Furthermore, as reported in the previous paper, there is still the separated decomposition of component at around 500 °C. The addition of both types of nanotubes reduces the decomposition temperature of the blend, to $T = 350$ °C which is in the "operating" range of the ability of the DB vapors to react with the polymer blend and quench the flame. Hence the addition of MWCNTs renders the blend flame-resistant and self-extinguishing under the UL-94 condition, whereas simply the addition of clays does not.

Cone Calorimetry. Flammability measurements were performed in the cone calorimeter, where the heat release rate (HRR) and the mass loss rate (MLR) represent that the heat is measured by measuring oxygen concentration in the exit gases, and that the mass is lost as a function of combustion times. The results form analysis of the data from the cone calorimetry experiments are tabulated in Table 3 and Table 4.

PMMA Homopolymers. From Figure 12, we can see that the peak HRR is 1440 kW/m^2 for the homopolymer. When FR particles are added, the peak is reduced to a steady plateau at about 490 kW/m^2. Similarly, in the absence of FR, a peak observed in the MLR which corresponds to the peak in the HRR. When the FR is added the MLR also becomes nearly constant in time. This large reduction of the PHRR by the addition of FR is not surprising and results primarily in chemical reactions as the FR particles go into the gas phase.[14] When only (0.5 wt %) of the *l*-MWCNTs are added in the PMMA/DB/AO nanocomposite, the flame retardant properties are not improved. In fact we can see that the time to ignition is decreased from 18 to around 10 s. Increasing the fractions of *l*-MSCNT to 1.5% does not alter the ignition time, and only slightly alters the MLR and HRR.

Kashiwagi et al. reported similar results for the PP/MWCNT systems where they also observed a sharp decrease

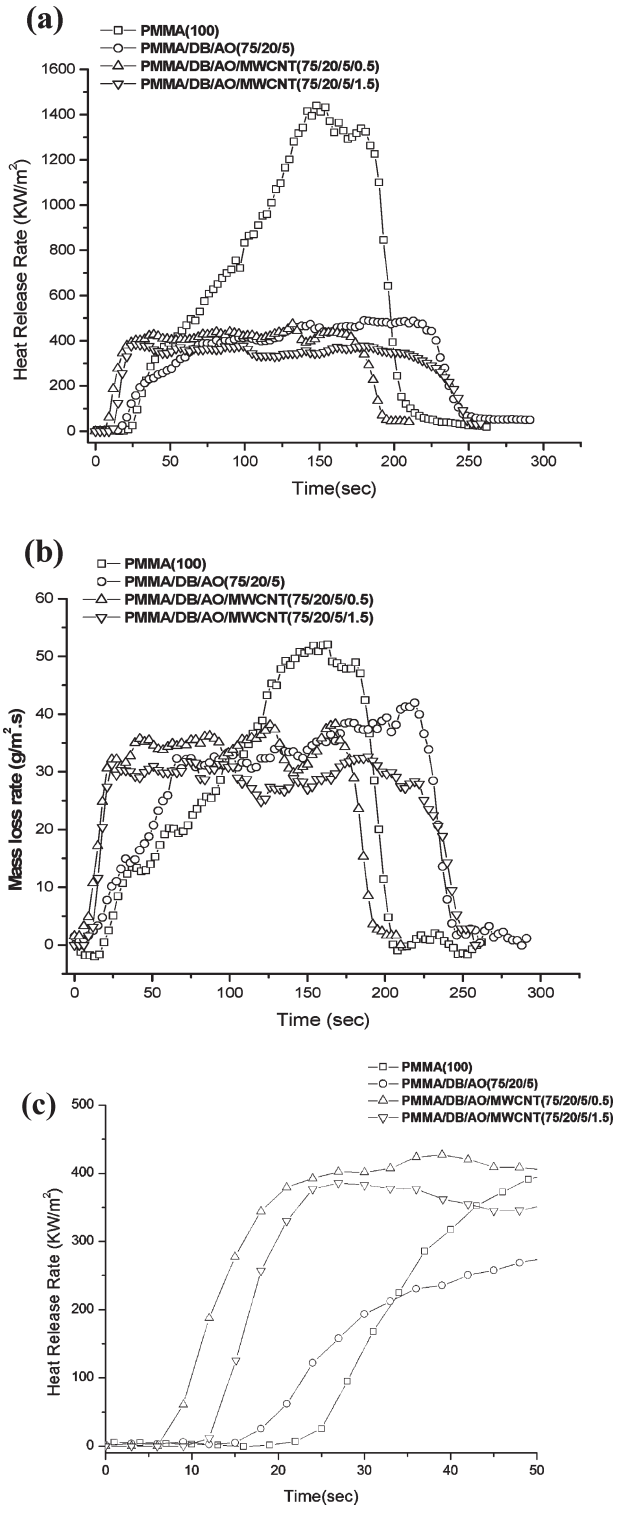

Figure 12. Effects of addition of *l*-MWCNT on HRR and MLR in PMMA/DB/AO(75/20/5) at 50 kW/m^2.

in the ignition time with only 0.5% MWCNT. When the MWCNT concentration was increased to 2% or higher, the time of ignition changed as well, and became more similar to the value of the unfilled PP. Rheological measurements performed on PMMA melts indicated that 2% was the percolation threshold for the formation of an entangled network of MWCNTs where physical contacts of the tubes was obtained.[3] We therefore postulate that these contacts are also effective at improving the thermal conductivity of

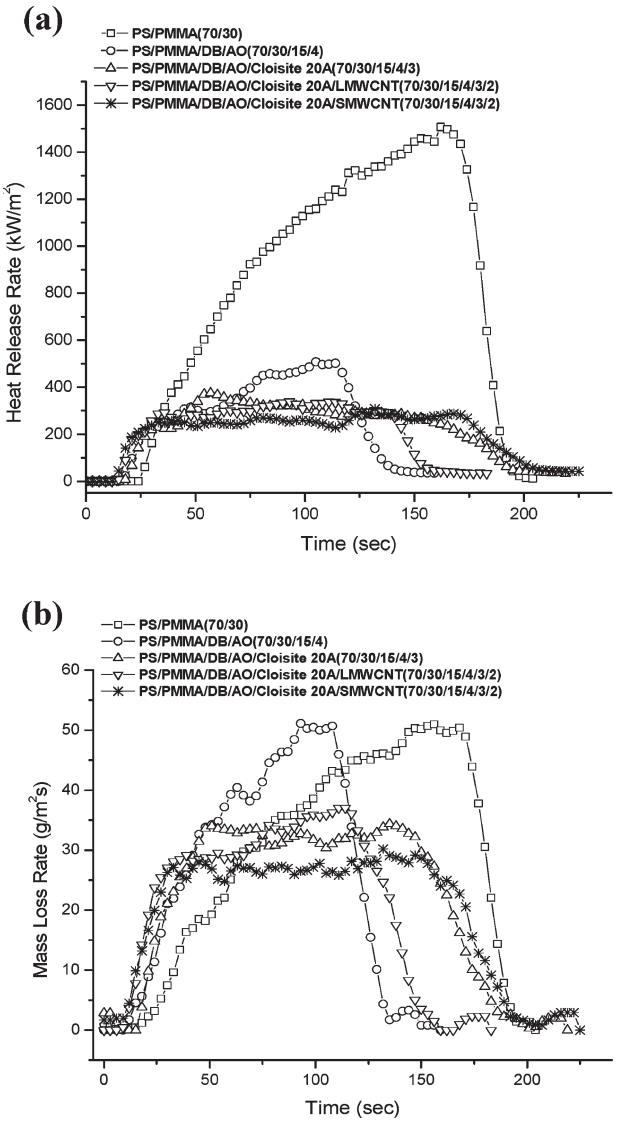

Figure 13. Effect of MWCNTs and clays additives in HRR and MLR of PS/PMMA/DB/AO at 50 kW/m^2.

the melts. The thermal conductivity of MWCNTs is 750 W/mK, which is much higher than that of clays or polymer, which are, respectively, 1.1 and 0.5 W/mK.[15−17] Hence when the concentration of MWCNTs is low, the tubes are surrounded only by the polymer matrix, which forms an insulating layer. As the thermal front advances, the tubes heat up faster than the surrounding polymer, igniting the matrix at earlier times. However, when the tubes are percolated, then they can also rapidly dissipate the heat throughout the sample, thereby potentially increasing the time to ignition.

PS/PMMA Polymer Blends. In Figure 13 we show the cone calorimetry data for PS/PMMA blends. From the figure we can see that in contrast to the PMMA melts, the addition of FR agents does not significantly improve the flame retardant properties. The FR agents decrease the peak HRR, but do not make a steady plateau at HRR. The addition of the FR increases the MLR and moves the peak to earlier times. The addition of only 3% Cloisite 20A produces the largest decrease in HRR and MLR. But as, previously reported, the blend is not self-extinguishing, according to the UL-94 V0 criteria. The addition of 2% MWCNTs and 3% Cloisite clays does produce the blend

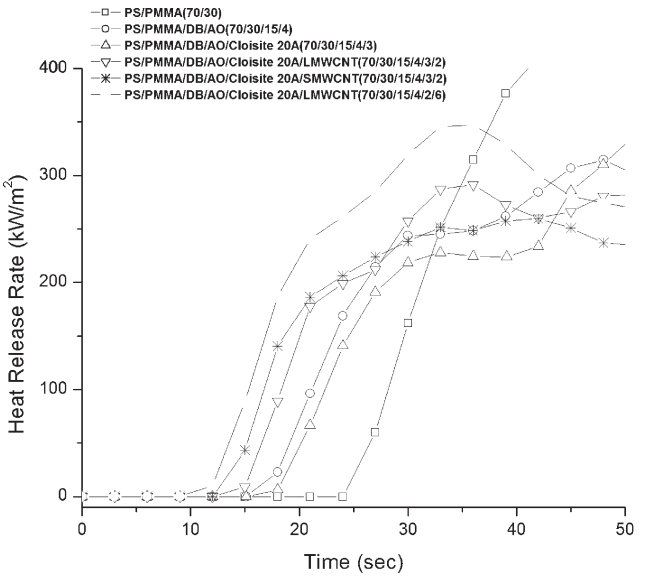

Figure 14. Effect of addition of MWCNTs and clays on time of ignition in HRR at 50 kW/m^2.

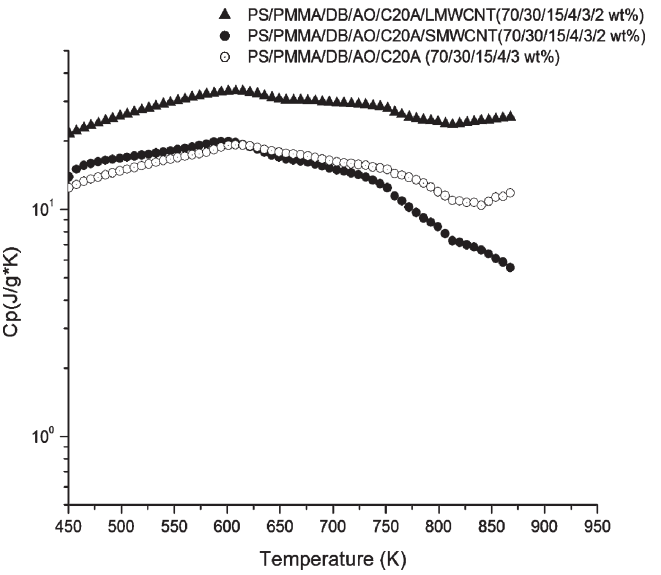

Figure 15. Comparison of specific heat C_p of three different chars as a function of temperature: (1) PS/PMMA/DB/AO/C20A, unfilled circle; (2) PS/PMMA/DB/AO/C20A/*l*-MWCNT, filled triangle; (3) PS/PMMA/DB/AO/C20A/*s*-MWCNT, filled circle.

which passed the UL-94 V0, but as can be seen from Figure 13, the thermal properties of two types of MWCNTs are different. The short nanotubes appear to be the most effective at reducing the MLR and HRR, while the long MWCNTs produce results which are worse than those of the clays alone.

In Figure 14, we show the times to ignition, where we find that the clays decreases the time of ignition, but both types of MWCNTs decrease it even more. Increasing the MWCNTs concentration even to 6% fails to further increase the ignition time. This is in sharp contrast to the PMMA melts, where 6% is far above the percolation concentration in a homopolymer-MWCNT matrix. From Figure 6 we found that both clays and MWCNTs were segregated preferentially in the PMMA phase. Hence we postulate that in this case the clays may be interfering with the contacts between the tubes achieved at a percolation. Hence the effective percolation may be occurring at even higher concentrations.

Analysis of Char. Neither PS nor PMMA form char when burned. A formation of rigid chars when functionalized clays are added to either the homopolymer or the blend may be one of the most important factors explaining in the large reduction of HRR and MLR. The formation of chars sets up a thermal barrier which dissipates heat from the burning gases and the external heat flux. We have previously shown that when the surfactants on the clays disintegrate, the clays form the long ribbon-like structures and in the case of the blends, even tube-like structures, which enhanced the thermal dissipation through contacts between the clay surfaces. The higher thermal conductivity of MWCNTs can, in principle, also improve the thermal properties of chars, if good physical contacts are achieved between the tubes.

In Figure 15, we plot the specific heat, C_p is inversely proportional to thermal diffusivity, of the chars as a function of temperature. From the figure we can see that the C_p of the blend with long nanotubes is even higher than that of the blend without the MWCNTs. Furthermore, the C_p remains fairly constant with temperature. On the other hand, the C_p of the blend containing the short nanotubes, is initially the same as that of the blend with just the clays, but as temperature increases above 600 K, the C_p is sharply reduced. Comparing this data to the one in Figure 13 we find that the addition of *l*-MWCNTs also increases the MLR and HRR over the values of the samples containing just the clays, while the addition of *s*-MWCNT reduces these quantities. We can then propose the following model to explain the enhanced flame retardant properties achieved only with the addition of the short nanotubes.

In Figure 16, we show SEM images of the three types of chars. From the figure, we can see that the char with *l*-MWCNTs contains many clay platelets entangled among the MWCNTs. The clay platelets interfere with the ability of the MWCNTs to form good thermal contacts with each other which are required to dissipate the heat by conduction. Furthermore, we can see that both types of MWCNTs interfere with the production of the clay ribbons or tubes reported previously.[7] Hence the improvement in the HRR and MLR obtained by adding the clays is reduced when the *l*-MWCNT are added. As, we discussed previously, the long MWCNTs are entangled and remain fairly stationary within the polymer blend, while the *s*-MWCNTs are mobile and can segregate into different areas in the molten polymer blends. Examination of the char containing the *s*-MWCNT in Figure 16c shows that most of the nanotubes are now segregated from the clays and into separate clusters where they can improve the physical contacts with each other and conduct heat more efficiently. The model is confirmed from measurement of the C_p of the chars in Figure 15 where we find that the value for the one with s-MWCNTs is the lowest.

In summary, good heat dissipation is crucial in improving the flame retardant properties of materials. The low thermal conductivity of MWCNTs in a polymer matrix can be of advantage when good thermal contacts between the tubes are possible. At early stages, when the polymer matrix is present, the *l*-MWCNTs provide a better thermal pathway, which helps in raising the ignition time by conductively dissipating heat, while at longer times, the ability of the *s*-MWCNT to segregate allows more thermally conducting chars to form, thereby reducing the HRR and MLR. Hence a combination of the two types of MWCNTs would probably provide the best thermal properties.

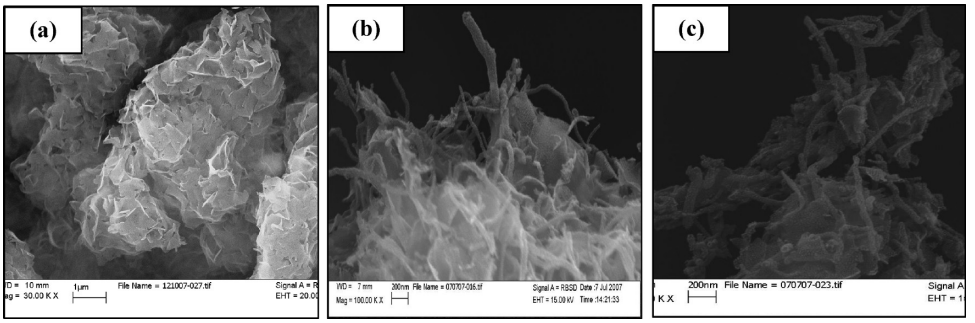

Figure 16. SEM images of chars: (a) PS/PMMA/DB/AO/C20A/l-MWCNTs; (b) PS/PMMA/DB/AO/C20A/l-MWCNTs; (c) PS/PMMA/DB/AO/C20A/s-MWCNTs.

4. Conclusion

We have shown that the addition of certain nanoparticles mixtures can enhance flame retardancy to a greater degree than the addition of either of the particles alone. The effect is particularly efficient in polymer blends, where more variables need be considered in the flame behavior. We studied PS/PMMA blends and the respective homopolymers. In this paper, we focused on the combination of MWCNTs with clays. We found that the FR particles segregate to the MWCNTs preferentially, thereby allowing the clays to segregate to the blend interfaces. In this manner, the clays are more efficient at stabilizing the blend against phase segregation during burning, while at the same time dispersing the FR particles uniformly. An important consideration in flame retardancy is the time to ignition as well as the HRR and MLR. Addition of either clays or MWCNTs can drastically lower the time to ignition, even though they have been shown to improve the HRR and MLR once ignition has started. The high thermal conductivity and low specific heat of the nanoparticles allows them to heat up faster than the surrounding polymer and reach the ignition temperature of the matrix sooner than the unfilled compound. If the nanoparticles form a percolating structure, such as that formed by the *l*-MWCNTs, which can entangle with each other, the heat is conducted away toward the sample surfaces, explaining the observation that with increasing concentration of the MWCNTs, the time to ignition increases (Figure 12 and ref 3.)

In the case of the blend, the situation is more complex. Here we also added clays to stabilize the compound against phase separation. The clays were interspersed between MWCNTs, preventing good contact, and as a result, no improvement in ignition time was observed even for concentrations as high as 6%, where percolation was shown to occur in homopolymers.[3] Even though the HRR and the MLR of the compounds containing *l*-MWCNTs and clays, were lower than those of the unfilled compound, they were higher than those of the compound containing only clays. The addition of short MWCNTs, on the other hand, did not affect the time to ignition but significantly reduced the HRR and the MLR. Prior to ignition, the *s*-MWCNTs were also separated by the clays, and had poor conduction properties, but as the polymer was heated, the *s*-MWCNTs became mobile, and we observed that they segregated together both in the char and in the compound. This resulted in a percolated phase which was able to reduce the specific heat at high temperatures. From these findings, we conclude the flame retardant properties of nanocomposites depend on the organization, as well as the chemical nature of nanoparticles. In this manner, combinations of nanoparticles can achieve a synergy which minimizes the total amount of fillers, and preserves the mechanical properties of polymer blends.

Acknowledgment. The authors thank Ms. Susan C. Van Horn from Central Microscopy Imaging Center (C-MIC) at Stony Brook University for taking TEM images. The authors also thank Prof. Edward Weil of Polytechnic University for reviewing and editing our initial manuscript and a revision. This work was supported by the NSF-MRSEC program, the AERTC through a grant from Brookhaven National Laboratory.

References and Notes

(1) Kashiwagi, T.; Du, F; Douglas, J; Winey, K. I.; Harris, R. H.; Shields, J. R. *Nat. Mater.* **2005**, *4*, 928–933.
(2) Kashiwagi, T.; Du, F; Douglas, J; Winey, K. I.; Groth, K. M.; Shields, J. R.; Bellayer, S. P.; KIM, H.; Douglas, J. F. *Polymer* **2005**, *46*, 471–481.
(3) Kashiwagi, T; Grulke, E.; Hilding, J.; Groth, K.; Harris, R.; Butler, K.; Shields, J.; Kharchenko, S.; Douglas, J. *Polymer* **2004**, *45*, 4227–4239.
(4) Kashiwagi, T.; Mu, M; Winey, K. I.; Cipriano, B.; Raghavan, S.; Pack, S.; Rafailovich, M.; Yang, Y.; Grulke, E.; Shields, J.; Harris, R.; Douglas, J *Polymer* **2008**, *49*, 4358–4368.
(5) Si, M.; Goldman, M.; Rudomen, G.; Gelfer, M. Y.; Sokolov, J. C.; Rafailovich, M. H. *Macromol. Mater. Eng.* **2006**, *291*, 602–611.
(6) Si, M.; Zaitsev, V.; Goldman, M.; Frenkel, A; Peiffer, D. G.; Weil, E.; Sokolov, J. C.; Rafailovich, M. H. *Polym. Degrad. Stab.* **2007**, *92*, 86–93.
(7) Pack, S.; Si, M.; Koo, J.; Sokolov, J. C.; Koga, T.; Kashiwagi, T.; Rafailovich, M. H. *Polym. Degrad. Stab.* **2009**, *93*, 306–326.
(8) Morgan, A. B.; Harris, R. H.; Kashiwagi, T.; Chyall, L. J.; Gilman, J. W. *Fire Mater.* **2002**, *26*, 247–253.
(9) Jang, B. K.; Wilkie, C. A. *Polymer* **2005**, *46*, 2933–2942.
(10) Si, M.; Araki, T.; Ade, H.; Kilcoyne, A. L. D.; Fisher, R.; Sokolov, J. C.; Rafailovich, M. H. *Macromolecules* **2006**, *39*, 4793–4801.
(11) Hu, X.; Zhang, W.; Si, M.; Gelfer, M.; Hsiao, B.; Rafailovich, M.; Sokolov, J.; Zaitsev, V.; Schwarz, S. *Macromolecules* **2003**, *36*, 823–829.
(12) Koo, J.; Shin, K.; Seo, Y.; Koga, T.; Park, S.; Satija, S.; Chen, X.; Yoon, K.; Hsiao, B.S.; Sokolov, J.C.; Rafailovich, M.H. *Macromolecules,* **2007**, *40*, 9510–9516.
(13) Zhang, Y.; Ge, S.; Tang, B.; Rafailovich, M. H.; Sokolov, J. C.; Peiffer, D. G.; Li, Z.; Dias, A. J.; McElrath, K. O.; Satija, S. K.; Lin, M. Y.; Nguyen, D. *Langmuir* **2001**, *17*, 4437–4442.
(14) Georlette, P.; Simons, J. Halogen-Containing Fire-Retardant Compounds. In *Fire Retardancy of Polymeric Materials*; Grand, A. E., Wilkie, C. A., Eds.; Marcel Dekker, Inc.: New York, 2000; pp 246−254.
(15) *Polymer Handbook*, 4th ed.; Brandrup, J., Immergut, E. H., Grulke, E. A., Eds.; Wiley: New York, 1999.
(16) *Handbook of Chemistry and Physics*, 70th ed.; Weast, R. C., Lide, D. R., Astle, M. J., Beyer, W. H., Eds.; CRC Press, Inc.: Boca Raton, FL, 1989−1990.
(17) Xie, H.; Cai, A.; Wang, X. *Phys. Lett. A* **2007**, *369*, 120–123.
(18) Si, M.; Hefter, J.; Song, A.; Rafailovich, M. H.; Sokolov, J. C. *J. Adhes. Sci. Technol.* **2005**, *19*, 1459–1474.
(19) Bao, S. P.; Tjong, S. C. *Mater. Sci. Eng., A* **2008**, *485*, 508–516.